Article

Morphological, Photoluminescence, and Electrical Measurements of Rare-Earth Metal-Doped Cadmium Sulfide Thin Films

Muhammad Azhar, Ghazi Aman Nowsherwan, Muhammad Aamir Iqbal, Saira Ikram, Azqa Farrukh Butt, Mohsin Khan, Naushad Ahmad, Syed Sajjad Hussain,* Muhammad Akram Raza, Jeong Ryeol Choi,* Saira Riaz, and Shahzad Naseem

Read Online

ACCESS | Metrics & More | Article Recommendations

ABSTRACT: This work is aimed at investigating the viability of utilizing cadmium sulfide (CdS) as a buffer layer in CdTe solar cells by analyzing and assessing its optical, photoluminescence, morphological, and electrical properties. These films were fabricated using a thermal coating technique. Optical microscopy was used to observe the changes in morphology resulting from the doping of rare-earth metals such as samarium (Sm) and lanthanum (La) to CdS, while the granular-like structure of the sample was confirmed by scanning electron microscopy. The objective of incorporating Sm and La ions into CdS was to enhance photoconductivity and optimize the optical bandgap, aiming to create a viable charge transport material for photovoltaic devices with enhanced efficiency. Through that process, a noticeable decrease in transmission, from approximately 80 to 68% in the visible region, was observed. Additionally, the bandgap value was reduced from 2.43 to 2.27 eV. Furthermore, during the analysis of the photoluminescence spectra, it was observed that emission peaks occurred in the visible region. These emissions were attributed to electronic transitions that took place via band-to-band and band-to-impurity interactions. The electrical measurements showed an enhancement in conductivity due to the decrease in the bandgap. This notable consequence of the doped materials suggests their utilization in photovoltaic systems.
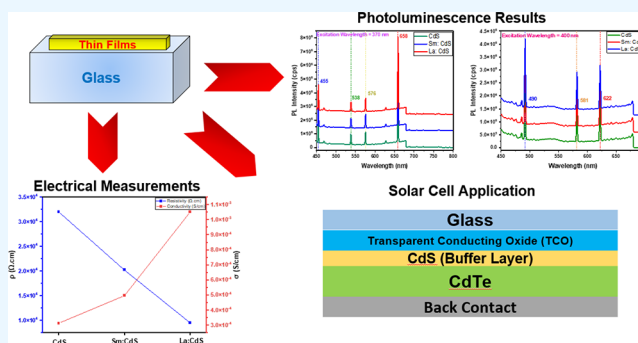
1. INTRODUCTION

Cadmium chalcogenides are a class of semiconducting materials composed of cadmium and chalcogen elements such as sulfur, selenium, or tellurium. These materials exhibit unique optical and electrical properties that make them attractive for various applications. CdS, cadmium selenide (CdSe), and cadmium telluride (CdTe) are the most commonly studied cadmium chalcogenides. They are extensively used in optoelectronic devices such as solar cells, photodetectors, and light-emitting diodes (LEDs) due to their tunable bandgaps and high absorption coefficients.[1−4] Additionally, cadmium chalcogenides are applicable to photocatalysis, sensors, and quantum dot technologies.[3−5] CdS nanostructures exhibit a direct bandgap value of 2.42 eV and an exciton binding energy of 28 mV at ambient temperature. These materials are widely used in fabricating optoelectronic devices and others, like photodetectors, photovoltaic (PV) devices, photocatalysis, and LEDs, due to their high transparency, strong photoconductivity, and low resistivity.[6−8] Many groups have recognized CdS's key properties with varied structures created by various deposition processes, such as spin-coating, chemical bath deposition, sol−gel, chemical

vapor deposition, thermal evaporation, RF sputtering, spray pyrolysis, and others.[9−16] In relation to this, thermal deposition is particularly important among all deposition processes because of its ease and low manufacturing cost on large-area substrates, while the required temperature is not so high.

In addition, CdTe stands out as one of the most promising materials for affordable photovoltaic applications. It has several advantages, including a nearly ideal bandgap for solar energy conversion (∼1.44 eV), a high absorption coefficient, and the ability to be deposited from solution, making it less expensive than many alternatives. The efficiency of CdTe solar cells can be further improved by integrating a buffer layer such as CdS,[17−19] which is the most commonly used buffer layer material in CdTe solar cells owing to its suitable energy band alignment with CdTe, as well as its stability and flexibility in

deposition. Despite its numerous advantages, the utilization of CdS as a buffer layer faces lots of challenges. Some of these challenges lie in the relatively wide bandgap of CdS, its low conductivity, and improper band alignment. This presents a drawback when it comes to the absorption of blue light, ultimately leading to a reduction in the overall efficiency of the device, but its properties can be tuned by the incorporation of rare-earth metals.

The doping mechanism is the most popular method for modifying semiconductors' structural, morphological, optical, and electrical characteristics. Sm and La have been shown to have an essential role in altering the critical optoelectrical characteristics of numerous semiconductor materials, including CdO, TiO$_2$, ZnS, and ZnO.[20−23] The significant difference in radius and charge between rare-earth trivalent ions (RE^{3+}) and divalent cadmium ions (Cd^{2+}) often impedes the successful integration of RE^{3+} into CdS, resulting in suboptimal energy transfers. Although the characteristics of many nanoparticles infused with lanthanide ions have been documented, yet a majority of them should be synthesized using high-temperature methods.[24,25] This synthesis typically results in particles devoid of organic groups on their surfaces. Notably, these rare-earth ions can potentially produce blue, green, and red hues, which are good for comprehensive color devices.

In past studies, CdS films doped with rare-earth elements such as terbium, ytterbium, praseodymium, neodymium, and europium have also been documented.[26−29] Semiconductor nanoparticles enriched with lanthanide ions offer notable benefits, especially in the realm of fluorescence labeling. These ions facilitate multicolor imaging using a single-wavelength excitation by harnessing diverse ions. Lanthanide ions are characterized by their extended lifetimes, making them invaluable for time-sensitive methods. Their presence also considerably mitigates the photobleaching that has been typically observed in fluorescent molecules. Rare-earth ion-based semiconductor materials have piqued the attention of researchers due to their half-filled outermost shell, which yields enhanced optoelectronic properties. Such properties lead to promising applications of rare materials in diverse disciplines, like LEDs, flat panel displays, photocatalysis, and PV devices.[30−32] The trivalent samarium ions, in particular, have garnered attention due to their impressive fluorescence efficiency in both visible and infrared spectra.[33] A comprehensive grasp of the optical characteristics of Sm^{3+} ions is crucial given their prospective technological applications.[34] A special focus has been put on Sm and La ions since they are excellent activator dopants and offer effective emission spectra. Saravanan et al. examined the physical properties of Sm-doped CdS nanostructures prepared by the coprecipitation method and observed significant morphology and structural changes caused by incorporating Sm in the CdS nanostructure.[35] Yang et al. studied the physical properties of La-doped CdS nanostructures prepared by the coprecipitation method and observed morphology and structural changes after incorporating La in the CdS nanostructure.[36]

Karthika et al. synthesized a TiO$_2$−ZrO$_2$ composite doped with CdS:Sm (3 wt %) nanostructures through the sol−gel method and examined the thermal as well as optical properties of the fabricated materials, leading to observing changes in the structural arrangement and improvements in optical results.[37] Shkir et al. prepared and characterized Sm-doped CdS nanostructures by spray pyrolysis and demonstrated their high performance in photodetector applications.[38] Abdel

Hameed and El Radaf synthesized La-doped CdS on a glass substrate by using the chemical bath deposition technique. They found that the transmittance declined from 80% by increasing the concentration of La, and the bandgap decreased from 2.45 to 2.09 eV by increasing the concentration from 0 to 12%.[39] Mathew and colleagues have delved into the optical[40] and dielectric properties[41] of II−VI/RE (Sm^{3+}) within sol−gel silica glasses, produced using the sol−gel technique. In contrast to surface-altered semiconductor nanoparticles, the RE-infused II−VI semiconductor nanocrystals display a distinctly sharp emission line. They also showcase a considerable gap between excitation and emission, along with an extended fluorescence lifetime. These features arise from transitions taking place within the incompletely filled 4f-shells of the RE ions. In addition, Yilmaz et al. studied the electrical, structural, and optical characteristics of Sm-doped CdS thin films prepared by spray pyrolysis: They found that these films exhibit the best optical results when Sm doped in CdS thin layers is 3% and exhibit optimum electrical characteristics when the doped Sm is 1%.[42]

Through this research, we seek to understand the optical and photoluminescence properties of CdS films, especially when they are doped with rare-earth metals like Sm and La. Our main objective is to determine whether such doped CdS films could effectively serve as a buffer layer and, in connection with that purpose, we find how to enhance the performance and efficiency of CdTe-based solar cells. Furthermore, an in-depth analysis of the morphological and electrical attributes is conducted, revealing their potential appropriateness for diverse optoelectronic applications. The insights derived from this research hold significant promise for enabling the development of innovative devices and understanding their functional mechanisms, thus acting as an invaluable guide for devising efficient production processes for related materials.

2. EXPERIMENTATION AND CHARACTERIZATION

2.1. Preparation of Thin Films. Here, we explored the process of thin film preparation through thermal evaporation using an Edward Coating's Unit 306. This system leverages the principles of high-vacuum thermal heating, wherein a resistive heat surface comes into contact with the source material, causing it to evaporate. It is possible to demonstrate the potentiality of this process from Figure 1, which represents its graphical design.

For the deposition of thin films, we utilized glass substrates as a base for CdS and rare-earth metal-doped CdS. In preparation, we meticulously cleaned the glass substrate to ensure the absence of dust or debris, which could potentially impact results. Initially, we manually scrubbed the glass slides with a detergent, followed by submerging them in acetone and isopropyl alcohol (IPA) solution for 15 min using an ultrasonic bath. To further eradicate persistent organic pollutants and adhering particles, we finally subjected the slides to a nitrogen spray. CdS nanopowder, utilized as the source material for thermal evaporation, was procured from Unichem China. On the other hand, Sm and La were sourced from Wanfeng Technology. We applied a process to deposit thin films using these materials. The weight of 0.25 g of CdS was taken for the operation. Alongside this, other compounds, X(Sm, La):CdS, with "X" representing either Sm or La, were also prepared. We ensured that X accounted for precisely 3% of the weight of this compound, with a total weight of 0.25 g. These prepared materials were then placed in a tungsten boat, a vessel designed
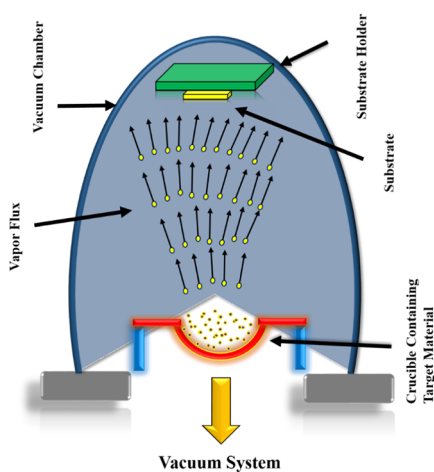
Figure 1. Schematic representation of thermal evaporation mechanism.

to endure high temperatures, which is an essential part of our process. The deposition itself was carried out using the highly reliable Edward Coater, which was maintained at a pressure of roughly 2×10^{-5} Torr and a current of 51 A.

2.2. Characterizations. We conducted an analysis of the crystal structure of the deposited thin films by using an X-ray diffraction technique that utilizes Cu Kα radiation with a wavelength of 1.5406 Å. The data produced in this process were recorded using a Bruker D8 Advance Diffractometer. For the assessment of chemical bonding and the quality of the material, we employed Fourier transform infrared spectroscopy (FTIR) using the Agilent Cary 630 FTIR Spectrometer. This technique typically records spectra between 650 and 4000 cm^{-1}, with the resultant signal serving as a unique identifier or "fingerprint" of the sample. We studied the optical parameters of the deposited samples using the UV−vis Shimadzu 1800 to investigate the interaction between electromagnetic waves and matter. The spectrum ranged from 200 to 1200 nm, and the distribution of light intensity in that range revealed transmission, absorption, and bandgap details. The photoluminescence (PL) properties of the thin films were analyzed using the FS5 spectrofluorometer, and this provided information about the material's excitation spectrum, emission spectrum, bandgap, and chromaticity across a spectrum of 200 to 1000 nm. We then examined the microstructure of the thin films using a NOVEX Holland optical microscope equipped with an integrated CCD camera at a magnification level of 1000×. This equipment uses lenses and visible light to magnify microscopic samples, which are then captured by conventional light-sensitive cameras. To explore the surface texture of the films, we utilized a scanning electron microscope (SEM), which employs a fixated electron beam that scans across the surface. The resultant secondary or backscattered electron signals produce highly detailed images of surface topography and depth of field, facilitating the assessment of surface roughness. Lastly, we implemented the Van der Pauw (VDP) method to measure voltage and current around the sample boundary, which yielded the thin film's mobility, average resistivity, and Hall coefficient parameters. This technique allows for the investigation of both regular and random patterns.

3. RESULTS AND DISCUSSIONS

3.1. Structural Analysis. The XRD patterns provide valuable information about the crystal structure and lattice parameters of the material. The obtained data were indexed using an analytical procedure that associates them with a standard reference pattern from the Xpert high score library. Figure 2 displays the XRD spectra of as-deposited and annealed
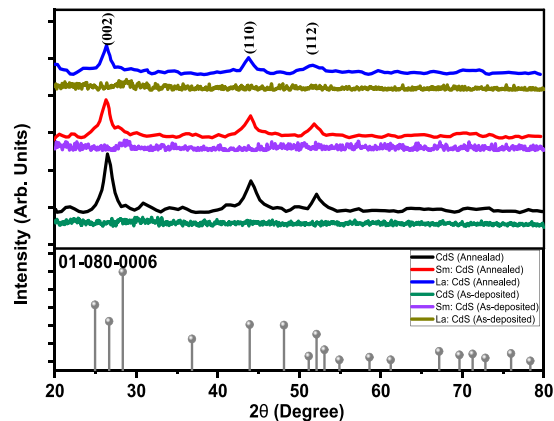
Figure 2. XRD patterns of CdS nanopowder and deposited thin films of CdS, Sm:CdS, and La:CdS.

CdS and doped-CdS thin films. Annealing was carried out at 300 °C in order to induce crystallinity in thin films. As can be seen from the XRD patterns, the as-deposited CdS and rare-earth metal-doped thin films (Sm:CdS and La:CdS) exhibit an amorphous nature due to lattice disorientation and the amorphous nature of the glass substrate and dopants.[43,44] The properties of glass, like its amorphous structure and built-in stresses due to doping, make it less conducive for crystal growth. An amorphous structure, like that of glass, lacks the long-range order present in crystalline materials. The doped materials may have built-in stresses due to the differences in atomic size and bonding behavior between the host material and the dopants. These stresses can create strain in the material and disrupt its ability to form a crystalline lattice.

As the thin film samples underwent annealing at a temperature of 300 °C, distinct peaks were evident in the diffractograms. These peaks manifested at 2θ values of 26.67, 43.90, and 52.11°, corresponding to the (002), (110), and (112) diffraction planes of the hexagonal wurtzite lattice of CdS (JCPDS no. 01-080-0006),[45,46] as illustrated in Figure 3. A notable increase in the intensity of these peaks indicates enhanced crystallinity in the film. The observation underscores the pivotal role of annealing temperature and conditions in dictating the structural and compositional properties of the film. Annealing can lead to the reduction of defects, impurities, and voids in the film. This results in smoother, more uniform films. The annealing process can relieve residual stresses in the film. These stresses might have been introduced during the deposition process. Relieving these stresses can prevent film cracking, delamination, and other forms of mechanical degradation. Furthermore, if the amorphous film is doped with certain elements to modify its properties, annealing can activate these dopants and facilitate their distribution within the film. These outcomes suggest that the annealing temperature and conditions significantly impact the structural and compositional characteristics of the film, with potential
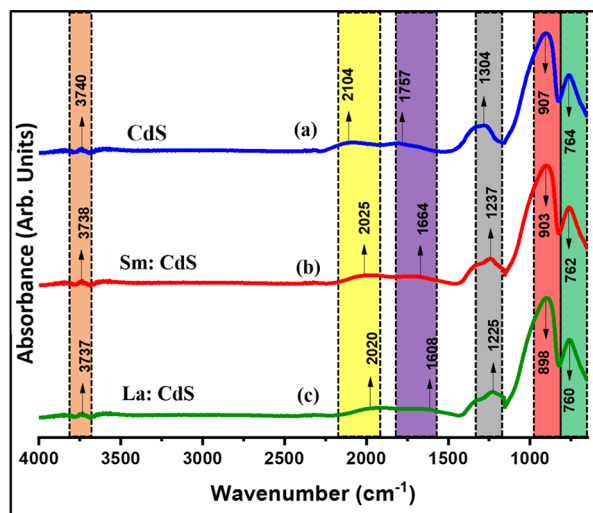
Figure 3. FTIR spectra. (a) CdS, (b) Sm:CdS, and (c) La:CdS thin films.

implications for its performance and use in various applications.

The diffractograms, while showcasing identifiable peaks characteristic of CdS, do not present any indications of the presence of metallic Sm or La nor their respective complex oxides. Meanwhile, a slight shift in peak positions, together with variation in peak intensity and peak width, is observed in the rare-earth metal CdS thin films, in contrast to the peaks of undoped CdS films. This shift toward lower angles can be attributed to the ionic radii of the doping elements. Specifically, the ionic radii for Sm^{3+} and La^{3+} stand at 0.96 and 1.03 Å, respectively. In comparison, the host Cd^{2+} has a marginally greater ionic radius of 0.97 Å. Introducing dopants with a larger ionic radius tends to exert structural strain within the CdS lattice, typically of the magnitude of 10^{-3}.[47] This structural strain, originating from tensile stresses due to the integration of foreign atoms into the crystal lattice, results in the expansion of the CdS lattice.[48] Additionally, the high charge state of the dopant has the potential to modify the concentration of sulfur vacancies in the CdS lattice, contingent on their specific location. Such dopants might occupy positions in the lattice interstitials, which in an undoped case would have been occupied by Cd^{2+} ions. One distinct observation drawn from the attached figure is the modulation in the intensity of the reflection peaks of the doped CdS films, signifying an improvement in their crystalline quality.

To determine the particle size, one can utilize the full-width half-maximum (FWHM) value obtained from the experimental data. FWHM is related to the particle size, crystalline nature, and wavelength of X-ray radiation used, and it can also be calculated using the Debye–Scherrer formula. The Debye–Scherrer formula can be uniquely expressed as (see ref 49):

$$D = K\lambda / \beta \cos \theta \tag{1}$$

where D represents the mean crystallite size, λ is the wavelength of the copper target that was used, β represents the FWHM of the peak, and θ is the diffraction angle. From XRD analysis, the average grain sizes of CdS, Sm:CdS, and La:CdS thin films were determined to be 7.49, 8.20, and 8.36 nm, respectively. The introduction of rare-earth ions into the CdS matrix can result in local lattice strain due to the difference in atomic sizes between the CdS host atoms and the

rare-earth dopants. The presence of this strain can lead to a higher density of defects, such as vacancies and interstitials. When the doped films undergo annealing, these defects can act as energy sources, promoting grain growth. Annealing processes typically increase the atomic mobility of the film. When combined with doping, this enhanced mobility facilitates the diffusion of dopant atoms into the CdS lattice. This, in turn, can promote grain boundary migration and Ostwald ripening, wherein smaller grains dissolve and contribute to the growth of larger grains, leading to an increase in average grain size.[50]

3.2. FTIR Spectroscopy Analysis. The analysis of X(Sm, La)-doped CdS thin films via an FTIR spectrometer provided insights into their chemical bonding. The vibrational mode of the deposited thin films is depicted in Figure 3. This figure shows characteristic FTIR spectra peaks within the 650–4000 cm^{-1} range. A faint absorption band was detected at 3740 cm^{-1}, attributed to the OH stretching vibration from moisture and water molecules present in the treated samples. A broad peak at 2104 cm^{-1} suggested a strong interaction between CdS and water, consistent with the stretching vibration of the −OH bond. Furthermore, a standard vibration band of CO ions was observed at 1304 cm^{-1}. The distinct peaks observed at 764 and 1757 cm^{-1} can be attributed to the bending vibration of CdS. Their presence confirms the successful formation of CdS within the sampled deposits.[51,52] The spectral analysis also reveals a prominent Si−O absorption peak, which is discernible around the wavenumber of 1304 cm^{-1}. Additionally, the range between 2000 and 2300 cm^{-1} showcases an absorption band that is typically associated with the stretching vibrations of Si−H and Si−H$_2$.[53] These bands are likely indicative of the glass substrate's influence on the spectrum, suggesting that the substrate's characteristics may have played a role in these observed absorptions. Further examination revealed noticeable changes in peak intensity and width upon the addition of Sm and La, signifying the influence of these elements on the CdS lattice. As depicted in Figure 3, the incorporation of these rare-earth metal elements appeared to induce a shift toward higher wavenumbers in the corresponding peaks. This shift suggests alterations in the bond length and molecular mass due to the interaction of rare-earth metal elements with CdS.

3.3. Optical Microscopy. Pure and rare-earth metal-doped CdS thin films were morphologically analyzed using an optical microscope to better understand the uniformity and structure of the deposited film (see Figure 4). As observed in Figure 4a, CdS was uniformly coated onto a glass substrate, and the particles were distributed across the entire surface, resulting from a vacuum-generated material and heating process designed to smooth the surface. Figure 4b,c depict how the surface morphology of the doped thin films changed with
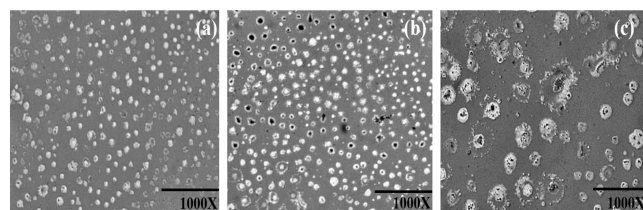
Figure 4. Optical micrographs at a magnification scale of 1000×. (a) CdS, (b) Sm:CdS, and (c) La:CdS.
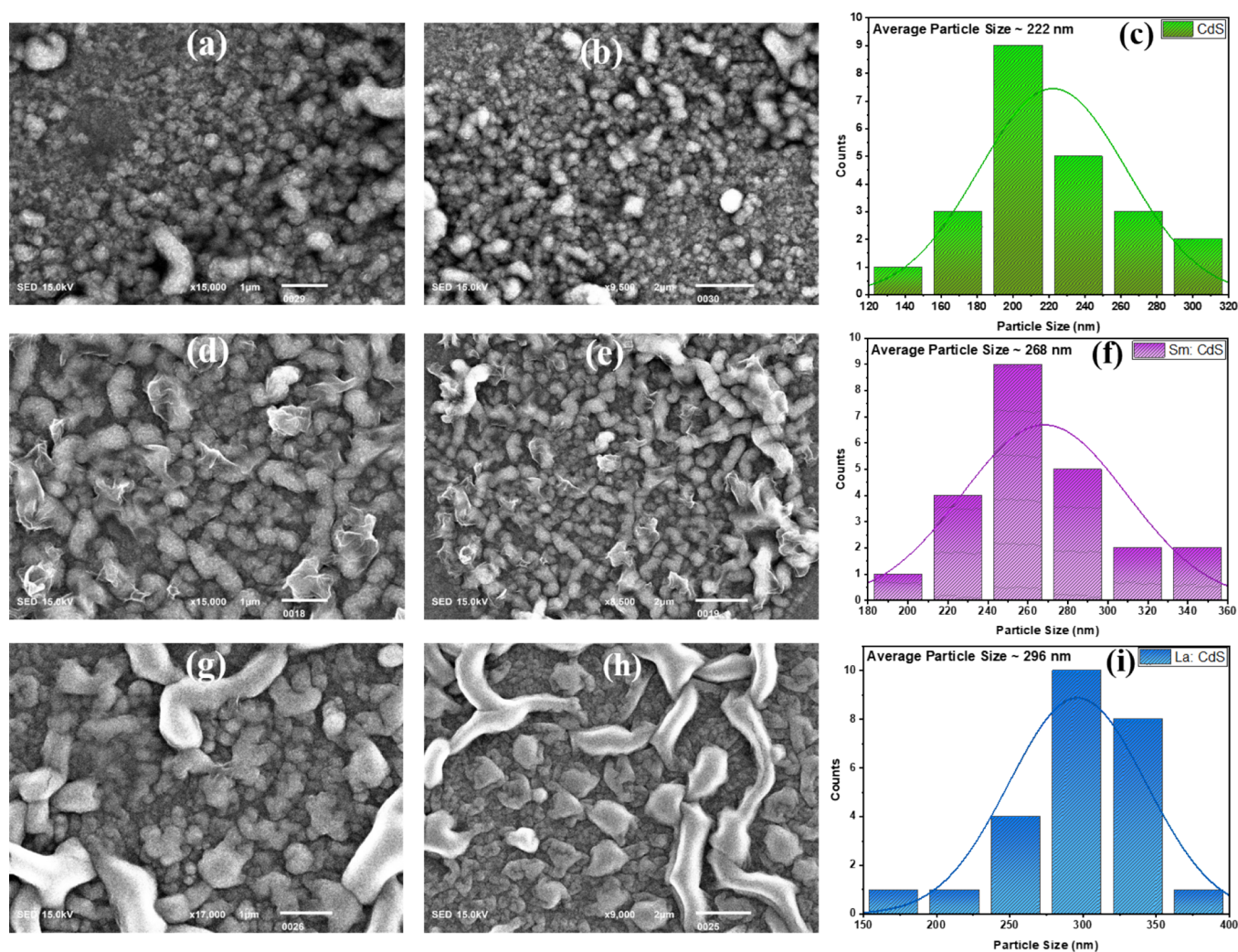
Figure 5. (a, d, g) SEM micrographs of CdS, Sm:CdS, and La:CdS at a magnification of 1 μm while (b, e, h) SEM micrograph of CdS, Sm:CdS, and La:CdS at a magnification of 2 μm. (c, f, i) Histogram of particle size variation of CdS, Sm:CdS, and La:CdS.

increasing Sm and La doping components, whereas pure CdS films appeared white. Moreover, we observed particle accumulation and an increase in Sm and La concentrations, which led to the formation of black spots in the micrographs.

3.4. Morphological Analysis. The morphological examination was conducted at various magnifications using a SEM at an accelerating voltage of 15 kV. These images of thermally evaporated CdS and X(Sm, La):CdS thin films are presented in Figure 5a,b,d,e,g,h. The images indicate that the resultant thin films have a thick morphology that extends across the entire glass substrate and are composed of spherical shapes resembling grains with no discontinuities. Particle size histograms are shown in Figure 5c,f,i. Particle sizes were estimated using the 1 μm magnification parameter in ImageJ program. The thin films of CdS, Sm:CdS, and La:CdS exhibited particle agglomeration on their surfaces with mean particle sizes of 222, 268, and 296 nm, respectively. The change in grain size could be attributable to the integration of Sm and La into the CdS lattice, which could also be responsible for influencing the electrical and optical characteristics of the thin films. It could be due to the nucleation of new crystal domains and/or promoting the growth of existing ones. This results in larger and more well-defined crystal structures, leading to an increase in particle size. The doping of transition

metals can influence the thermodynamics of the thin film system, leading to an Ostwald ripening effect. This means that smaller particles dissolve, and the material composed of those particles is redeposited onto larger particles, causing them to grow in size. Furthermore, it also enhances the diffusion of material on the film surface. This increased mobility of atoms allows for more effective coalescence and agglomeration of particles, leading to larger particle sizes.

3.5. Elemental Analysis. EDX spectroscopy was employed to find the elemental composition of the deposited thin films. The position or energy of a peak in the EDX spectrum directly corresponds to one of these characteristic X-ray energies of specific elements. Thus, the peak position or energy in an EDX spectrum serves as a fingerprint for elemental identification. In our spectrum, each colored dot signifies distinct elements found within the deposited thin films. The quantitative spectrum analysis, in terms of weight percentage, indicates 26.43% for Cd and 23.59% for S in the case of the CdS thin film. For the Sm:CdS thin film, we found 38.56% for Cd, 35.42% for S, and 2.89% for Sm, while for La:CdS thin film, the analysis showed 36.47% for Cd, 32.16% for S, and 2.74% for La, as can be demonstrated from Figure 6. The remaining percentage in the EDX spectrum is attributed to carbon and oxygen atoms. The emergence of a relative peak for
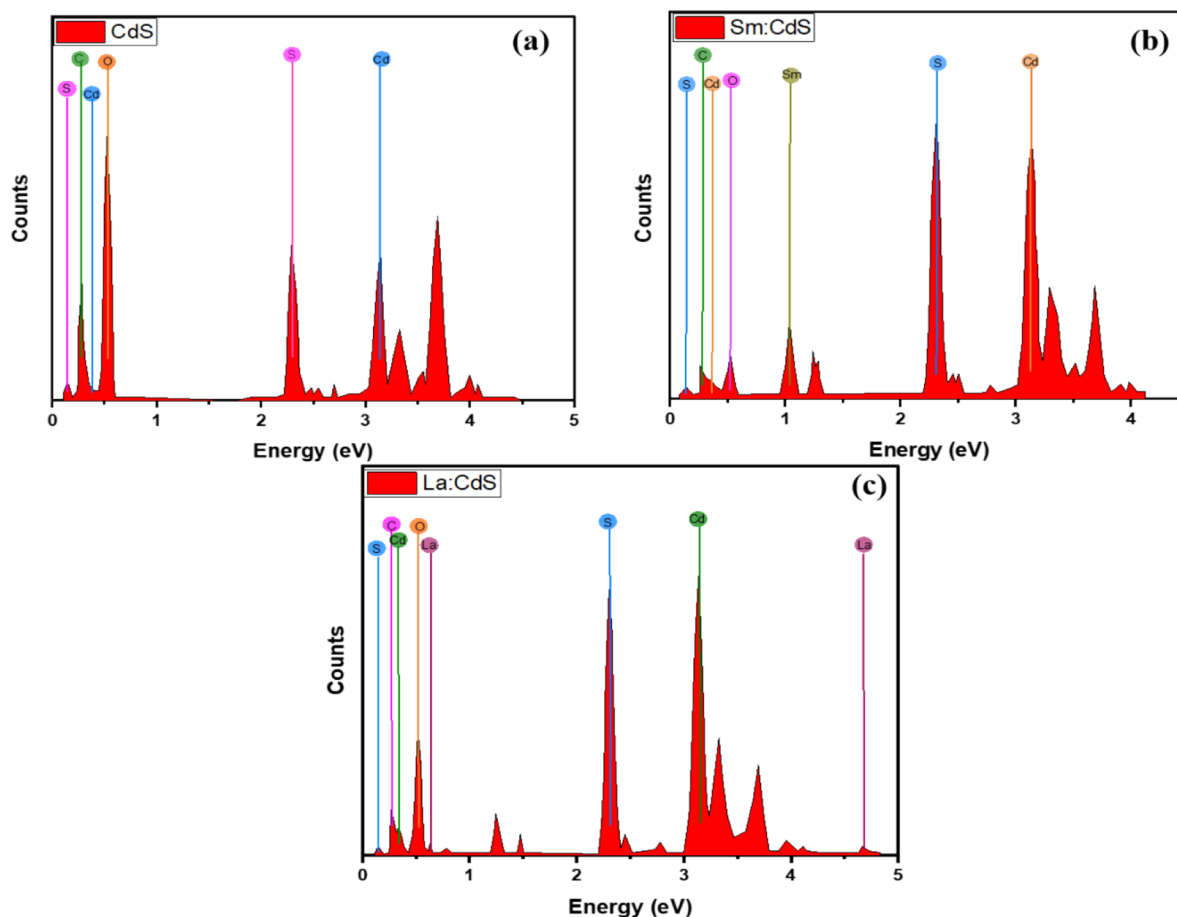
Figure 6. EDX spectra. (a) CdS, (b) Sm:CdS, and (c) La:CdS thin films.

carbon and oxygen in the EDX spectrum can be attributed to the presence of surface contamination at the interface. In the spectrum, the intensity of a peak is proportional to the number of atoms of that element excited by the incident beam. The peak area in an EDX spectrum is indicative of the amount or concentration of a specific element in the sample. The correlation varies depending on the atom type, the beam intensity, and the depth of penetration. Rare-earth metals have been detected in CdS thin films using EDX spectroscopy with no additional dopants detectable in the CdS thin film.

3.6. UV−vis Spectroscopy. To investigate the optical properties of the deposited samples, a UV spectrophotometer was employed, covering a range of 250−1200 nm. Figure 7 presents the transmission (see Figure 7b) and absorption spectra (see Figure 7a) of both CdS and rare-earth metal-doped CdS thin films. The results show a significant level of transmission in the visible and near-infrared regions while demonstrating minimal transmission in the UV region. Oscillations in the transmission spectra could be attributed to thin film effects caused by light interference, a typical occurrence in films prepared by thermal evaporation. We also confirmed a potential impact of incorporating Sm and La into CdS on the fundamental absorption edge; that is, the absorption edge specifically shifted toward longer wavelengths. The maximum transmittances of approximately 80, 73, and 68% were found at a wavelength of around 580 nm for CdS, Sm:CdS, and La:CdS thin films, respectively. As a consequence, the rare-earth metal-doped CdS could be applicable not only to the analysis of electron transport but

also as the buffer layer of PV devices. The transmission spectrum of the film suggests that its surface is smooth and uniform.

To estimate the energy of the optical bandgap, Tauc plots were employed. These plots provide a relationship between the square of the product of the absorption coefficient (α) and photon energy ($h\nu$), plotted against energy (eV). The energy value can be calculated using the following formula:[54]

$$\alpha h\nu = A(h\nu - E_g)^{1/2} \tag{2}$$

$$E_g = 1242/\lambda \tag{3}$$

where λ denotes the wavelength. The optical bandgap values for CdS, Sm:CdS, and La:CdS thin films are displayed in Figure 7c, utilizing the linear extrapolating method. The as-deposited CdS thin film exhibited a measured bandgap value of 2.43 eV. After introducing rare-earth metal doping, the optical bandgap decreased slightly from 2.43 to 2.27 eV. This shift can be attributed to structural modifications occurring within the CdS film due to the incorporation of rare-earth metal elements. The decrease in bandgap is likely associated with energy level localization and band-tailing effects resulting from the wave function overlap between electrons and impurity atoms.[55,56]

3.7. Photoluminescence Spectroscopy. The FS5 spectrofluorometer, featuring a xenon arc lamp as an excitation source, was employed to examine the PL properties of the deposited samples. Photoluminescence serves as an effective approach for confirming electronic transitions in nano-structured semiconductor materials. Altering the excitation
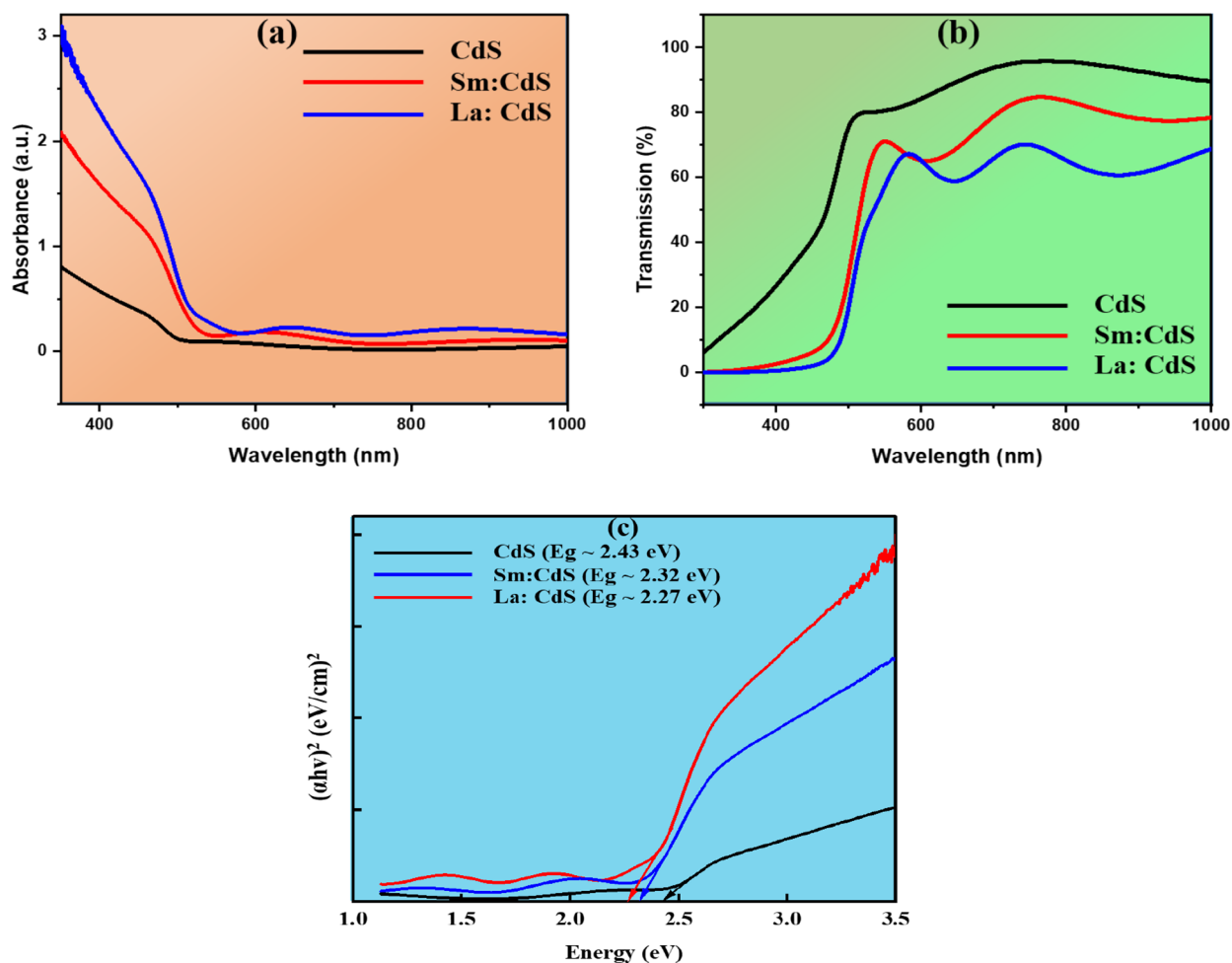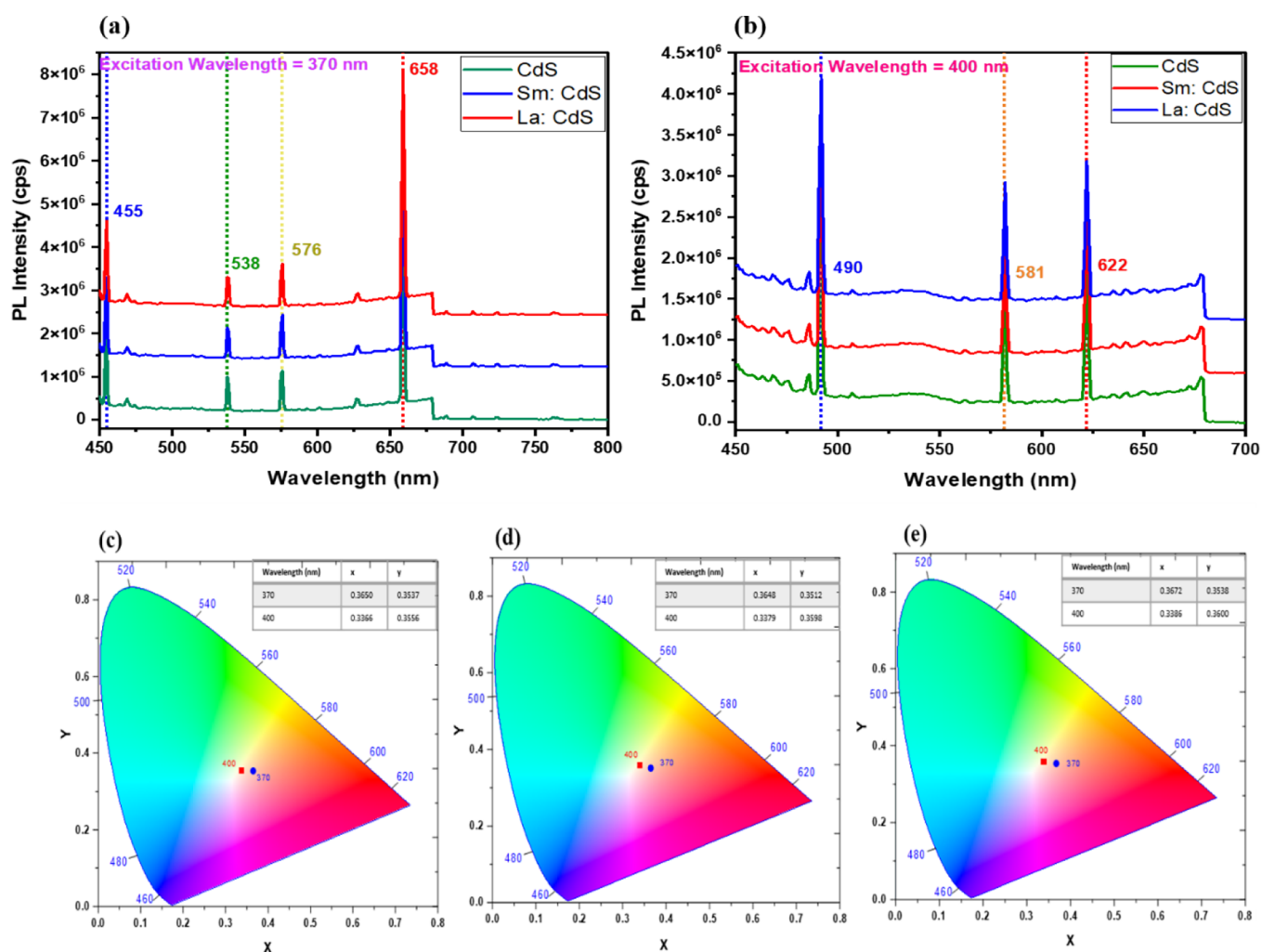
Figure 7. (a) Absorbance spectra of CdS, Sm:CdS, and La:CdS thin films, (b) transmission (%) spectra of CdS, Sm:CdS, and La:CdS thin films, and (c) Tauc plot of CdS, Sm:CdS, and La:CdS thin films.
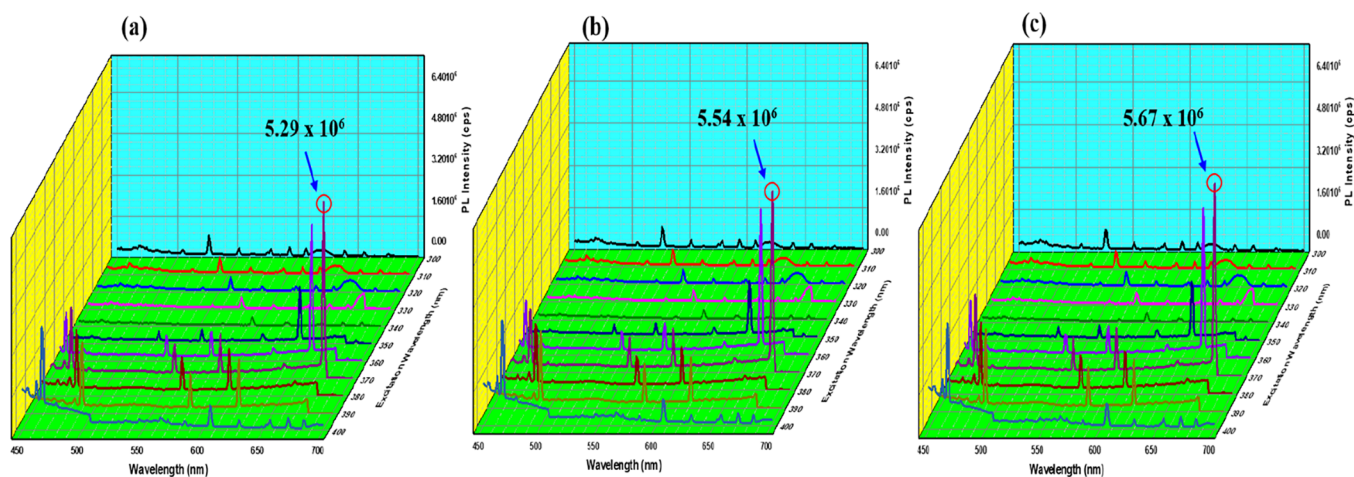
Figure 8. Excitation map. (a) CdS, (b) Sm:CdS, and (c) La:CdS thin films from 300 to 400 nm of wavelength.

wavelength results in a change in the resulting emission spectrum. The PL spectra of CdS and doped-CdS thin films are analyzed in Figure 8a−c. The experimentation revealed a notable relationship between excitation wavelength and emission intensity for the examined CdS and doped-CdS thin films. The collected data conclusively showed that the emission intensity exhibited an increasing trend in line with the excitation wavelength. The peak emission intensity was

observed at an excitation wavelength of 370 nm. The highest emission intensities, measured at a wavelength of 658 nm, for the CdS, Sm:CdS, and La:CdS samples were 5.29×10^6, 5.54×10^6, and 5.67×10^6, respectively. These results, which can be extracted from Figure 8, distinctly confirm the dependence of emission intensity on the excitation wavelength in these particular thin films.

Figure 9. PL spectra of CdS, Sm:CdS, and La:CdS thin films at an excitation wavelength of (a) 370 nm and (b) 400 nm, chromaticity plots. (c) CdS, (d) Sm:CdS, and (e) La:CdS thin films at 370 and 400 nm of wavelength.

In PL spectroscopy, the intensity of photoemission refers to the amount of light emitted by a material when it is excited by a photon of a particular wavelength. If the excitation wavelength increases, the energy of the exciting photon decreases, and, thereby, the photoemission intensity generally increases. The absorption efficiency of a material typically decreases with increasing photon energy (or decreasing wavelength). This means that as the excitation wavelength increases, more photons are absorbed by the material, leading to a higher population in excited states. Consequently, a large number of electrons in the excited states implies nothing but more electrons being available for recombination and subsequent emission of photons, thereby increasing the photoemission intensity. When the excitation wavelength is longer (lower energy), it may be closer to the bandgap energy, leading to a lower probability of exciting electrons across this energy barrier. As a result, fewer electrons are available for recombination, decreasing the photoemission intensity. In some cases, the emitted photons have a lower energy (longer wavelength) than the absorbed photons. This is known as the Stokes shift. When the excitation wavelength is longer, it reduces the energy mismatch between the absorbed and emitted photons. As a result, more energy is transferred to the lattice vibrations or other nonradiative processes. The slight variation in peak intensity and peak broadness can be

demonstrated in Figure 8. It could be due to the incorporation of rare-earth metals in CdS thin films. It is important to note that the relationship between the excitation wavelength and the photoemission intensity can vary depending on the specific properties of the material being studied. These factors include the electronic structure, energy levels, and the presence of defects or impurities, among others.

Figure 9a,b depicts the typical PL spectra of CdS thin film excited at 370 and 400 nm, respectively. The PL spectra visually illustrate the emission peaks predominantly falling within the visible spectrum. Notably, the peak observed at 538 nm corresponds to the transition from donor energy levels to the valence band. Additionally, the peak at 576 nm is likely attributed to traps or surface states. The depicted samples exhibited band edge emission around 455 nm, and this is a phenomenon resulting from the recombination of excited electrons that become trapped at shallow levels, forming bound electron–hole pairs. On the other hand, the peak at 658 nm is associated with sulfur vacancies induced by doping, occurring at the transition level.[57,58] The significant peak observed at 490 nm may arise from interband transitions, which could result from sulfur-vacancy donors transitioning to the valence band and donor–acceptor recombination. The peak at 581 nm is likely influenced by interstitial defects present in the material. Furthermore, the PL spectra exhibit a distinct red emission
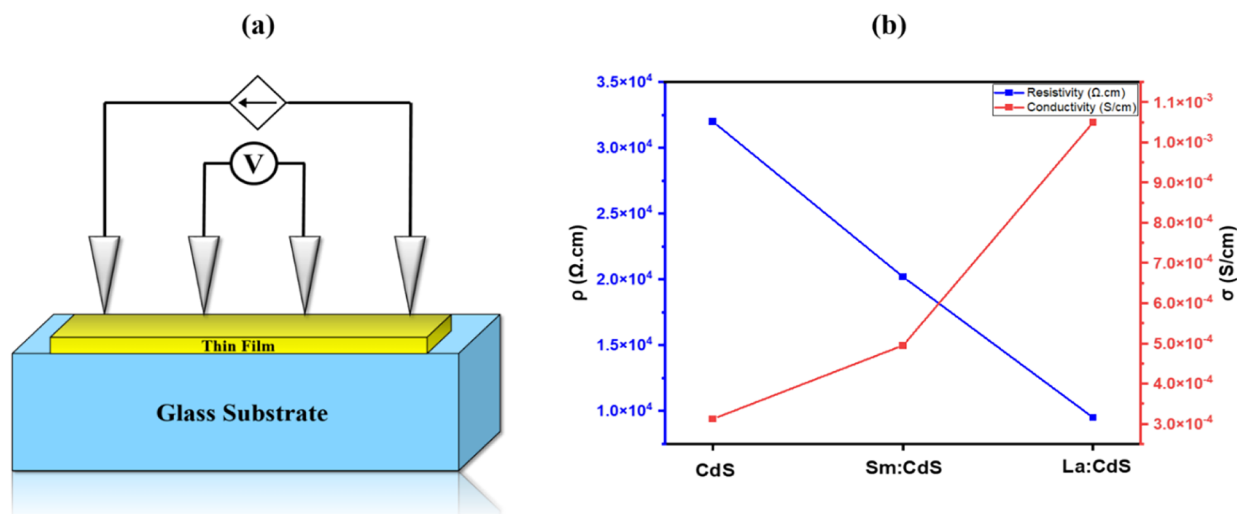
Figure 10. (a) Diagrammatic representation of the four-probe method and (b) resistivity along with conductivity plot of deposited thin films.

band at 622 nm, which is strongly correlated with sulfur vacancies caused by doping-induced defects. This emission band is commonly associated with the transition level.[59,60]

A notable near-band edge (NBE) peak, located between 500 and 700 nm, is evident and likely due to an interband transition or the recombination of electrons and holes. The NBE emission peak intensity and broadness increase with the integration of Sm and La, indicating the presence of structural defects within the CdS lattice. As the concentration of rare-earth metals in the CdS system increases, so does the strength of the NBE peak.[60,61] The low intensity of emission peaks suggests a low concentration density of optically activated Sm and La ions. The red emission is attributed to sulfur (V_S) and cadmium vacancies (V_{Cd}, I_{Cd}). As La content is added to the CdS lattice, the red emission peak increases. La-doped films have a greater red emission intensity. This suggests that in addition to V_{Cd} and I_{Cd}, the La^{+3} ions contribute more to intrinsic defects. Sm^{+3} and La^{+3} ions likely occupy interstitial positions rather than replacing Cd, causing Sm and La-doped samples to have significant defect levels. Additionally, the presence of Sm^{+3} and La^{3+} ions in the samples further improves the lifetime of excitons. This improvement is achieved through the synergistic effect of an optimal concentration of dopants and the corresponding crystal defects, which facilitate the efficient transfer and trapping of photoexcited charges. Therefore, rare-earth metal doping may be a crucial factor in modifying the emission characteristics of CdS films.

Figure 9c−e showcases a chromaticity diagram that provides a visual representation of the visible spectrum by utilizing deposited thin films, which result in producing various hues. This diagram suggests that the material in question holds potential for applications in optoelectronic devices. Chromaticity, which represents all possible spectral colors and their combinations based on different values of the three primary colors (blue, green, and red), is depicted on a two-dimensional $X-Y$ plane, illustrating hue and saturation. If we introduce a three-dimensional representation, the "Z" axis would control color brightness. The corners of the triangle in the diagram represent the three primary colors: green, red, and blue. As the curve of the triangle approaches its center, the colors become less vibrant, ultimately representing white. In deposited thin films, white light has been emitted from different coordinates on excitation at various wavelengths. In the center of the

diagram, white light is achieved by properly combining colors with specific intensities at wavelengths of 460 nm (blue), 520 nm (green), and 680 nm (red). This chromaticity diagram enables geometric analysis effectively, leading us to predict the outcome of the additive mixing of two or more colored lights.

3.8. Electrical Measurements. The resistivity of CdS thin films and rare-earth metal-doped CdS thin films has been assessed using the four-probe method. The schematic representation of the four-probe method is illustrated in Figure 10a. This method is based on observing voltage changes between two locations (inner two locations in Figure 10a) while 1 mA current flows across another two locations (outer two locations in Figure 10a), where a magnetic field of 0.2 T was applied to several areas. Using this method, the average resistivity is calculated. The mean resistivity values for CdS, Sm:CdS, and La:CdS have been recorded as 3.2×10^4, 2.11×10^4, and 9.5×10^3 ohm-cm, respectively. Figure 10b shows the effects of doping materials on resistivity and conductivity, and it has been observed that CdS displays a higher resistivity compared to doped-CdS thin films. This pattern is supported by the incorporation of rare-earth metals into CdS. As resistivity decreases, conductivity increases, facilitating a smoother flow of charges across the material's surfaces. Such an increase in conductivity could be largely attributed to the narrowing of the bandgap by doping. The implications of these findings suggest potential applications of this material in solar technology, specifically as a buffer layer and an electron transport layer.

3.9. Application as a Buffer Layer in CdTe-Based Solar Cells. CdS thin films are used as buffer layers due to band alignment, passivation, preventing diffusion, and optical transparency.[62,63] The conduction band offset between CdS and CdTe is small, which means that electron transport from the CdTe to the CdS and eventually to the front contact is efficient. CdS can help to passivate the CdTe surface, reducing recombination at the CdTe/CdS interface and thus improving cell efficiency. A CdS layer can help to prevent the diffusion of atoms between the CdTe layer and the front contact, which can degrade device performance over time. It is also optically transparent in the visible region, which is important to ensure that light can reach the CdTe absorber layer. However, there are some challenges associated with the use of CdS as a buffer layer. CdS has a relatively wide bandgap of ∼2.4 eV, which can
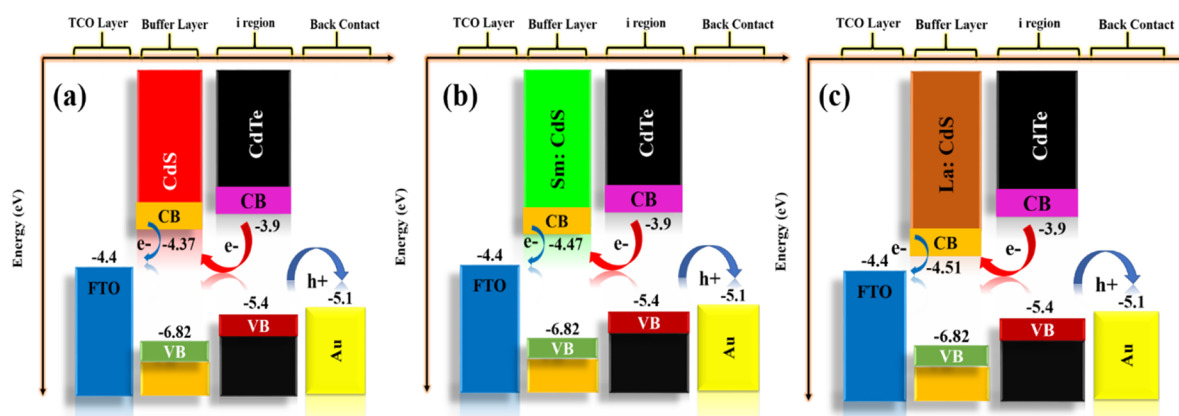
Figure 11. Energy band alignment of CdTe-based solar cells with the application of deposited thin films. (a) CdS, (b) Sm:CdS, and (c) La:CdS.

absorb blue light and decrease the overall device efficiency.[64−67]

On the other hand, the unique electronic structures of rare-earth metal elements are responsible for their special properties, which make them useful in a wide range of optoelectronic fields, including photovoltaics. While the use of such rare metals in solar cell technology is still not common, there has been some research regarding the use of rare-earth metal-doped buffer layers to enhance solar cell performance.[68−72] The introduction of rare-earth metal ions at the CdS/CdTe interface can modify the band alignment and improve charge separation and transport. The schematic of the energy band alignment of deposited thin films in CdTe-based solar cells is illustrated in Figure 11. Doping with certain rare-earth metal elements can tune the bandgap of CdS, potentially reducing the loss of blue photon energy and improving the overall efficiency of the device. Certain rare-earth metal elements can passivate defects in CdS, reducing recombination and improving device efficiency. These significant findings suggest the potential of rare-earth-doped CdS thin films to serve as effective buffers and electron transport layers in future solar cells. This could enhance solar cell efficiency, marking an important development in photovoltaic technology.

4. CONCLUSIONS

This study illustrated not only the successful deposition of CdS but also the doping of it with rare-earth metal thin films based on the thermal evaporation technique. Both UV−vis and PL spectroscopy were utilized to assess the optical characteristics of the samples. XRD and FTIR spectroscopy were employed to identify the crystal structure and the composition of the deposited materials. The influence of doping CdS with Sm and La on morphology was examined through optical microscopy and SEM. FTIR further established the identity of the material by showcasing unique peaks in the fingerprint region. Following the introduction of Sm and La, UV−vis spectroscopy demonstrated transmission rates of ∼70% in the visible spectrum and ∼ 80% in the infrared region, which is relatively low compared to undoped CdS thin films. The bandgap reduction is largely attributed to the introduction of Sm and La ions, whereas this reduction leads to band-tailing effects. In addition, PL spectroscopy revealed various emission peaks within the visible range, resulting from both direct and indirect recombination of electrons with holes. Notably, the electrical measurements indicated decreased resistivity and increased conductivity following the addition of Sm and La to the parent

material. These findings suggest the potential use of such rare-earth-doped semiconductor materials as buffer and electron transport layers in future solar cells with promising enhanced photovoltaic efficiency.

■ ASSOCIATED CONTENT

Data Availability Statement

All data generated or analyzed during this study are included in this published article.

■ AUTHOR INFORMATION

Corresponding Authors

Syed Sajjad Hussain − *Centre of Excellence in Solid State Physics, University of the Punjab, Lahore 54590, Pakistan;* Email: sajjadh.cssp@pu.edu.pk

Jeong Ryeol Choi − *School of Electronic Engineering, Kyonggi University, Suwon, Gyeonggi-do 16227, Republic of Korea;* Email: choiardor@hanmail.net

Authors

Muhammad Azhar − *Centre of Excellence in Solid State Physics, University of the Punjab, Lahore 54590, Pakistan*

Ghazi Aman Nowsherwan − *Centre of Excellence in Solid State Physics, University of the Punjab, Lahore 54590, Pakistan*

Muhammad Aamir Iqbal − *School of Materials Science and Engineering, Zhejiang University, Hangzhou 310027, China;* orcid.org/0000-0002-5031-5305

Saira Ikram − *Centre of Excellence in Solid State Physics, University of the Punjab, Lahore 54590, Pakistan*

Azqa Farrukh Butt − *Centre of Excellence in Solid State Physics, University of the Punjab, Lahore 54590, Pakistan*

Mohsin Khan − *Centre of Excellence in Solid State Physics, University of the Punjab, Lahore 54590, Pakistan*

Naushad Ahmad − *Department of Chemistry, College of Science, King Saud University, Riyadh 11451, Kingdom of Saudi Arabia*

Muhammad Akram Raza − *Centre of Excellence in Solid State Physics, University of the Punjab, Lahore 54590, Pakistan*

Saira Riaz − *Centre of Excellence in Solid State Physics, University of the Punjab, Lahore 54590, Pakistan*

Shahzad Naseem − *Centre of Excellence in Solid State Physics, University of the Punjab, Lahore 54590, Pakistan*

Complete contact information is available at:
https://pubs.acs.org/10.1021/acsomega.3c04936

Author Contributions

All authors have read and agreed to the published version of the manuscript.

Notes

The authors declare no competing financial interest.

■ REFERENCES

(1) Tsuji, M.; Aramoto, T.; Ohyama, H.; Hibino, T.; Omura, K. Characterization of CdS thin-film in high efficient CdS/CdTe solar cells. *Jpn. J. Appl. Phys.* **2000**, *39*, 3902.

(2) Zhao, J.; Bardecker, J. A.; Munro, A. M.; Liu, M. S.; Niu, Y.; Ding, I.-K.; Luo, J.; Chen, B.; Jen, A. K.-Y.; Ginger, D. S. Efficient CdSe/CdS quantum dot light-emitting diodes using a thermally polymerized hole transport layer. *Nano Lett.* **2006**, *6*, 463−467.

(3) Isshiki, M.; Wang, J. II-IV semiconductors for optoelectronics: CdS, CdSe, CdTe. In *Springer Handbook of Electronic and Photonic Materials* (pp. 1−1). Springer, Cham. 2017, DOI: 10.1007/978-3-319-48933-9_33.

(4) Wu, C.; Jie, J.; Wang, L.; Yu, Y.; Peng, Q.; Zhang, X.; Cai, J.; Guo, H.; Wu, D.; Jiang, Y. Chlorine-doped n-type CdS nanowires with enhanced photoconductivity. *Nanotechnology* **2010**, *21*, No. 505203.

(5) Liu, Y.; Shen, S.; Zhang, J.; Zhong, W.; Huang, X. Cu₂₋ₓSe/CdS composite photocatalyst with enhanced visible light photocatalysis activity. *Appl. Surf. Sci.* **2019**, *478*, 762−769.

(6) Tajima, S.; Umehara, M.; Hasegawa, M.; Mise, T.; Itoh, T. Cu₂ZnSnS₄ photovoltaic cell with improved efficiency fabricated by high-temperature annealing after CdS buffer-layer deposition. *Progr. Photovolt.: Res. Appl.* **2017**, *25*, 14−22.

(7) Morales-Acevedo, A. Thin film CdS/CdTe solar cells: research perspectives. *Solar Energy* **2006**, *80*, 675−681.

(8) Repins, I.; Contreras, M. A.; Egaas, B.; DeHart, C.; Scharf, J.; Perkins, C. L.; To, B.; Noufi, R. 19 9%-efficient ZnO/CdS/CuInGaSe² solar cell with 81 2% fill factor. *Progr. Photovolt.: Res. Appl.* **2008**, *16*, 235−239.

(9) Seon, J. B.; Lee, S.; Kim, J. M.; Jeong, H. D. Spin-coated CdS thin films for n-channel thin film transistors. *Chem. Mater.* **2009**, *21*, 604−611.

(10) Ziabari, A. A.; Ghodsi, F. E. Influence of Cu doping and post-heat treatment on the microstructure, optical properties and photoluminescence features of sol−gel derived nanostructured CdS thin films. *J. Lumin.* **2013**, *141*, 121−129.

(11) Memarian, N.; Rozati, S. M.; Concina, I.; Vomiero, A. Deposition of nanostructured CdS thin films by thermal evaporation method: effect of substrate temperature. *Materials* **2017**, *10*, 773.

(12) Uda, H.; Yonezawa, H.; Ohtsubo, Y.; Kosaka, M.; Sonomura, H. Thin CdS films prepared by metalorganic chemical vapor deposition. *Sol. Energy Mater. Sol. Cells* **2003**, *75*, 219−226.

(13) Punnoose, A.; Marafi, M.; Prabu, G.; El-Akkad, F. CdS thin films prepared by RF magnetron sputtering in Ar atmosphere. *Phys. Status Solidi A* **2000**, *177*, 453−458.

(14) Moualkia, H.; Hariech, S.; Aida, M. S. Structural and optical properties of CdS thin films grown by chemical bath deposition. *Thin Solid Films* **2009**, *518*, 1259−1262.

(15) Hiie, J.; Dedova, T.; Valdna, V.; Muska, K. Comparative study of nano-structured CdS thin films prepared by CBD and spray pyrolysis: annealing effect. *Thin Solid Films* **2006**, *511-512*, 443−447.

(16) Orlianges, J. C.; Champeaux, C.; Dutheil, P.; Catherinot, A.; Mejean, T. M. Structural, electrical and optical properties of carbon-doped CdS thin films prepared by pulsed-laser deposition. *Thin Solid Films* **2011**, *519*, 7611−7614.

(17) Reyes-Banda, M. G.; Regalado-Perez, E.; Pintor-Monroy, M. I.; Hernández-Gutiérrez, C. A.; Quevedo-López, M. A.; Mathew, X. Effect of Se diffusion and the role of a thin CdS buffer layer in the performance of a CdSe/CdTe solar cell. *Superlattices Microstruct.* **2019**, *133*, No. 106219.

(18) Kapadnis, R. S.; Bansode, S. B.; Supekar, A. T.; Bhujbal, P. K.; Kale, S. S.; Jadkar, S. R.; Pathan, H. M. Cadmium telluride/cadmium sulfide thin films solar cells: a review. *ES Energy Environ.* **2020**, *10*, 3−12.

(19) Romeo, A.; Artegiani, E. CdTe-based thin film solar cells: past, present and future. *Energies* **2021**, *14*, 1684.

(20) Robert Xavier, A.; Ravichandran, A. T.; Ravichandran, K.; Mantha, S.; Ravinder, D. Sm doping effect on structural, morphological, luminescence and antibacterial activity of CdO nanoparticles. *J. Mater. Sci.: Mater. Electron.* **2016**, *27*, 11182−11187.

(21) Hu, L.; Song, H.; Pan, G.; Yan, B.; Qin, R.; Dai, Q.; Fan, L.; Li, S.; Bai, X. Photoluminescence properties of samarium-doped TiO₂ semiconductor nanocrystalline powders. *J. Lumin.* **2007**, *127*, 371−376.

(22) Dehmukh, K.; Mukherjee, M.; Bhushan, S. Structural and optical studies on La doped CdS nanocrystalline films. *Turk. J. Phys.* **2012**, *36*, 9−21.

(23) Agrawal, S.; Khare, A. Effect of La on optical and structural properties of CdS−Se films. *Arabian J. Chem.* **2015**, *8*, 450−455.

(24) Saravanan, L.; Pandurangan, A.; Jayavel, R. Synthesis and luminescence enhancement of Cerium doped CdS nanoparticles. *Mater. Lett.* **2012**, *66*, 343−345.

(25) Zych, E.; Hreniak, D.; Strek, W. Spectroscopic properties of Lu₂O₃/Eu³⁺ nanocrystalline powders and sintered ceramics. *J. Phys. Chem. B* **2002**, *106*, 3805−3812.

(26) Das, S.; Mandal, K. C. Optical downconversion in rare earth (Tb³⁺ and Yb³⁺) doped CdS nanocrystals. *Mater. Lett.* **2012**, *66*, 46−49.

(27) Deng, L.; Shan, Y.; Xu, J. J.; Chen, H. Y. Electro-chemiluminescence behaviors of Eu³⁺-doped CdS nanocrystals film in aqueous solution. *Nanoscale* **2012**, *4*, 831−836.

(28) Linares-Avilés, M. E.; Contreras-Rascón, J. I.; Díaz-Reyes, J.; Martínez-Juárez, J.; Castillo-Ojeda, R. S.; Galván-Arellano, M.; Balderas-Lopez, J. A.; Álvarez-Ramos, M. Characterization of CBD-CdS Doped with Some Rare Earths III (Eu³⁺, Ce³⁺) as Function of Synthesis Time. *Mater. Res.* **2018**, *21*, No. e20170626.

(29) Yılmaz, S.; Polat, İ.; Tomakin, M.; Bacaksız, E. A research on growth and characterization of CdS:Eu thin films. *Appl. Phys. A* **2019**, *125*, 1−10.

(30) Wellenius, P.; Suresh, A.; Muth, J. F. Bright, low voltage europium doped gallium oxide thin film electroluminescent devices. *Appl. Phys. Lett.* **2008**, *92*, No. 021111.

(31) Devi, S. K. L.; Sudarsanakumar, K. Photoluminescent properties of Sm³⁺-doped zinc oxide nanostructures. *J. Lumin.* **2010**, *130*, 1221−1224.

(32) Wang, H. Q.; Batentschuk, M.; Osvet, A.; Pinna, L.; Brabec, C. J. Rare-earth ion doped up-conversion materials for photovoltaic applications. *Adv. Mater.* **2011**, *23*, 2675−2680.

(33) Lin, H.; Pun, E. Y. B.; Huang, L. H.; Liu, X. R. Optical and luminescence properties of Sm³⁺-doped cadmium−aluminum−silicate glasses. *Appl. Phys. Lett.* **2002**, *80*, 2642−2644.

(34) Němec, P.; Jedelský, J.; Frumar, M. On the effect of composition on the Judd−Ofelt parameters of Sm3+−doped chalcogenide glasses. *J. Non-Cryst. Solids* **2003**, *326-327*, 325−329.

(35) Saravanan, L.; Jayavel, R.; Pandurangan, A.; Jih-Hsin, L.; Hsin-Yuan, M. Influence of Sm doping on the microstructural properties of CdS nanocrystals. *Powder Technol.* **2014**, *266*, 407−411.

(36) Zhang, Y.; Fu, L.; Shu, Z.; Yang, H.; Tang, A.; Jiang, T. Substitutional doping for aluminosilicate mineral and superior water splitting performance. *Nanoscale Res. Lett.* **2017**, *12*, 456.

(37) Karthika, S.; Prathibha, V.; Ann, M. K. A.; Viji, V.; Biju, P. R.; Unnikrishnan, N. V. Structural and spectroscopic studies of Sm^{3+}/CdS nanocrystallites in sol−gel TiO_2-ZrO_2 matrix. *J. Electron. Mater.* **2014**, *43*, 447−451.

(38) Shkir, M.; Ashraf, I. M.; Khan, A.; Khan, M. T.; El-Toni, A. M.; AlFaify, S. A facile spray pyrolysis fabrication of Sm: CdS thin films for high-performance photodetector applications. *Sens. Actuators, A* **2020**, *306*, No. 111952.

(39) Abdelhameed, R. M.; El Radaf, I. M. Self-cleaning lanthanum doped cadmium sulfide thin films and linear/nonlinear optical properties. *Mater. Res. Express* **2018**, *5*, No. 066402.

(40) Mathew, S.; Rejikumar, P. R.; Adiyodi, A. K.; Jyothy, P. V.; Unnikrishnan, N. V. Structural and optical characterization of oxygenated CdTe/Sm^{3+} in sol−gel silica glasses. *Mater. Chem. Phys.* **2008**, *112*, 1061−1064.

(41) Mathew, S.; Rejikumar, P. R.; Yohannan, J.; Mathew, K. T.; Unnikrishnan, N. V. Microwave studies on the dielectric properties of Sm^{3+} and Sm^{3+}/CdTe doped sol−gel silica glasses. *J. Alloys Compd.* **2008**, *462*, 456−459.

(42) Yılmaz, S.; Polat, İ.; Tomakin, M.; Küçükömeroğlu, T.; Töreli, S. B.; Bacaksız, E. Sm-doped CdS thin films prepared by spray pyrolysis: a structural, optical, and electrical examination. *Appl. Phys. A* **2018**, *124*, 1−8.

(43) Vishwas, M.; Shamala, K. S.; Gandla, S. B. Comparison of optical properties of CdS thin films synthesized by spray pyrolysis and thermal evaporation method. *J. Opt.* **2022**, *51*, 736−740.

(44) Kathirvel, D.; Suriyanarayanan, N.; Prabahar, S.; Srikanth, S. Structural, electrical and optical properties of CdS thin films by vacuum evaporation deposition. *J. Ovonic Res.* **2011**, *7* ().

(45) Kumar, S.; Sharma, J. K. Stable phase CdS nanoparticles for optoelectronics: a study on surface morphology, structural and optical characterization. *Mater. Sci.-Pol.* **2016**, *34*, 368−373.

(46) Nowsherwan, G. A.; Zaib, A.; Shah, A. A.; Khan, M.; Shakoor, A.; Bukhari, S. N. S.; Riaz, M.; Hussain, S.; Shar, M. A.; Alhazaa, A. Preparation and Numerical Optimization of TiO_2:CdS Thin Films in Double Perovskite Solar Cell. *Energies* **2023**, *16*, 900.

(47) Sakthivel, P.; Asaithambi, S.; Karuppaiah, M.; Sheikfareed, S.; Yuvakkumar, R.; Ravi, G. Different rare earth (Sm, La, Nd) doped magnetron sputtered CdO thin films for optoelectronic applications. *J. Mater. Sci.: Mater. Electron.* **2019**, *30*, 9999−10012.

(48) Pan, L. L.; Li, G. Y.; Lian, J. S. Structural, optical and electrical properties of cerium and gadolinium doped CdO thin films. *Appl. Surf. Sci.* **2013**, *274*, 365−370.

(49) Shakoor, A.; Nowsherwan, G. A.; Alam, W.; Bhatti, S. Y.; Bilal, A.; Nadeem, M.; Zaib, A.; Hussain, S. S. Fabrication and characterization of TiO_2: ZnO thin films as electron transport material in perovskite solar cell (PSC). *Phys. B* **2023**, *654*, No. 414690.

(50) Khajuria, S.; Sanotra, S.; Ladol, J.; Sheikh, H. N. Synthesis, characterization and optical properties of cobalt and lanthanide doped CdS nanoparticles. *J. Mater. Sci.: Mater. Electron.* **2015**, *26*, 7073−7080.

(51) Esakkiraj, E.; Kadhar, S. P. S. A.; Henry, J.; Mohanraj, K.; Kannan, S.; Barathan, S.; Sivakumar, G. Optostructral and vibrational characteristics of Cu:CdS nanoparticles by precipitation method. *Optik* **2013**, *124*, 5229−5231.

(52) Islam, M. A.; Haque, F.; Rahman, K. S.; Dhar, N.; Hossain, M. S.; Sulaiman, Y.; Amin, N. Effect of oxidation on structural, optical and electrical properties of CdS thin films grown by sputtering. *Optik* **2015**, *126*, 3177−3180.

(53) Jana, S.; Das, S.; Gangopadhyay, U.; Mondal, A.; Ghosh, P. A clue to understand environmental influence on friction and wear of diamond-like nanocomposite thin film. *Adv. Tribol.* **2013**, *2013*, 1.

(54) Petrus, R. Y.; Ilchuk, H. A.; Kashuba, A. I.; Semkiv, I. V.; Zmiiovska, E. O.; Honchar, F. M. optical properties of CdS thin films. *J. Appl. Spectrosc.* **2020**, *87*, 35−40.

(55) Awan, S. U.; Hasanain, S. K.; Aftab, M. Influence of Li^{1+} co-doping defects on luminescence and bandgap narrowing of ZnO: Co^{2+} nanoparticles due to band tailing effects. *J. Lumin.* **2016**, *172*, 231−242.

(56) Chandramohan, S.; Kanjilal, A.; Sarangi, S. N.; Majumder, S.; Sathyamoorthy, R.; Som, T. Effect of Fe-ion implantation doping on structural and optical properties of CdS thin films. *Appl. Phys. A* **2010**, *99*, 837−842.

(57) Chandekar, K. V.; Shkir, M.; Alshahrani, T.; Khan, A.; AlFaify, S. An in-depth investigation of physical properties of Nd doped CdS thin films for optoelectronic applications. *Chin. J. Phys.* **2020**, *67*, 681−694.

(58) Islam, M. A.; Hatta, S. F. W. M.; Misran, H.; Akhtaruzzaman, M.; Amin, N. Influence of oxygen on structural and optoelectronic properties of CdS thin film deposited by magnetron sputtering technique. *Chin. J. Phys.* **2020**, *67*, 170−179.

(59) Kim, D.; Park, Y.; Kim, M.; Choi, Y.; Park, Y. S.; Lee, J. Optical and structural properties of sputtered CdS films for thin film solar cell applications. *Mater. Res. Bull.* **2015**, *69*, 78−83.

(60) Murthy, K. V. R.; Virk, H. S. Luminescence Phenomena: An Introduction. *Defect Diffus. Forum* **2013**, *347*, 1−34.

(61) Dousti, M. R.; Ghoshal, S. K.; Amjad, R. J.; Sahar, M. R.; Nawaz, F.; Arifin, R. Structural and optical study of samarium doped lead zinc phosphate glasses. *Opt. Commun.* **2013**, *300*, 204−209.

(62) Dharmadasa, I. M.; Ojo, A. A. Unravelling complex nature of CdS/CdTe based thin film solar cells. *J. Mater. Sci.: Mater. Electron.* **2017**, *28*, 16598−16617.

(63) Khrypunov, G.; Vambol, S.; Deyneko, N.; Suchikova, Y. Increasing the efficiency of film solar cells based on cadmium telluride. *East.-Eur. J. Enterp. Technol.* **2016**, *6*, 12−18.

(64) Iqbal, M. A.; Ahmad, A.; Malik, M.; Choi, J. R.; Pham, P. V. Pressure-Induced Bandgap Engineering and Tuning Optical Responses of $Cd_{0.25}Zn_{0.75}S$ Alloy for Optoelectronic and Photovoltaic Applications. *Materials* **2022**, *15*, 2617.

(65) Iqbal, M. A.; Malik, M.; Shahid, W.; Din, S. Z.; Anwar, N.; Ikram, M.; Idrees, F. Materials for Photovoltaics: Overview, Generations, Recent Advancements and Future Prospects. *Thin Films Photovoltaics*. IntechOpen, 2022, DOI: 10.5772/intechopen.101449.

(66) Iqbal, M. A.; Malik, M.; Zahid, A.; Islam, M. R.; Arellano-Ramírez, I. D.; Al-Bahrani, M. Unveiling concentration effects on the structural and optoelectronic characteristics of $Zn_{1−x}Cd_xS$ (x= 0, 0. 25, 0.50, 0.75, 1) cubic semiconductors: a theoretical study. *RSC Adv.* **2022**, *12*, 22783−22791.

(67) Iqbal, M. A.; Malik, M.; Bakhsh, S.; Sohail, M.; Arellano-Ramírez, I. D.; Morsy, K. Theoretical Insights into Pressure-Driven Stability and Optoelectronic Response of $Cd_{0.75}Zn_{0.25}S$ Alloy for Blue−Violet Display. *Adv. Theory Simul.* **2023**, *6* (9), 2300270 DOI: 10.1002/adts.202300270.

(68) Zafar, M.; Kim, B.; Kim, D. H. Improvement in performance of inverted organic solar cell by rare earth element lanthanum doped ZnO electron buffer layer. *Mater. Chem. Phys.* **2020**, *240*, No. 122076.

(69) Nowsherwan, G. A.; Hussain, S. S.; Khan, M.; Haider, S.; Akbar, I.; Nowsherwan, N.; Ikram, S.; Ishtiaq, S.; Riaz, S.; Naseem, S. Role of graphene-oxide and reduced-graphene-oxide on the performance of lead-free double perovskite solar cell. *Zeitschrift für Naturforschung A* **2022**, *77*, 1083−1098.

(70) Khan, M.; Iqbal, M. A.; Malik, M.; Hashmi, S. U. M.; Bakhsh, S.; Sohail, M.; Qamar, M. T.; Al-Bahrani, M.; Capangpangan, R. Y.; Alguno, A. C.; Choi, J. R. Improving the efficiency of dye-sensitized solar cells based on rare-earth metal modified bismuth ferrites. *Sci. Rep.* **2023**, *13*, 3123.

(71) Iqbal, M. A.; Malik, M.; Anwar, N.; Bakhsh, S.; Javeed, S.; Maidin, S. S.; Morsy, K.; Capangpangan, R. Y.; Alguno, A. C.; Choi, J. R. Basic Concepts, Advances and Emerging Applications of Nanophotonics. *Arabian J. Chem.* **2023**, *16*, No. 105040.

(72) Chen, Z.; Li, Q.; Chen, C.; Du, J.; Tong, J.; Jin, X.; Li, Y.; Yuan, Y.; Qin, Y.; Wei, T.; Sun, W. Enhanced charge transport and photovoltaic performance induced by incorporating rare-earth phosphor into organic−inorganic hybrid solar cells. *Phys. Chem. Chem. Phys.* **2014**, *16*, 24499−24508.